Geochemistry Geophysics Geosystems G3

Published by AGU and the Geochemical Society

Article
Volume 12, Number 8
4 August 2011
Q08002, doi:10.1029/2011GC003558
ISSN: 1525-2027

Along-strike variations of earthquake apparent stress at the Nicoya Peninsula, Costa Rica, subduction zone

Jana Stankova-Pursley and Susan L. Bilek
EES Department, New Mexico Institute of Mining and Technology, 801 Leroy Place, Socorro, New Mexico 87801, USA (janas@ees.nmt.edu)

W. Scott Phillips
EES-11, Los Alamos National Laboratory, Los Alamos, New Mexico 87545, USA

Andrew V. Newman
School of Earth and Atmospheric Sciences, Georgia Institute of Technology, Atlanta, Georgia 30332, USA

[1] Oceanic plates vary in temperature, topography, and sediment load as they enter subduction zones. These variations persist along the subduction interface causing perturbations in coupling and earthquake rupture processes. We explore the effects of variable subducting plate structure on microseismicity rupture characteristics along the Nicoya Peninsula, Costa Rica. The subducting Cocos Plate has low relief along the northern and central portion of the peninsula, with seamounts present at the southern tip of the peninsula. We compute apparent stresses for 94 M_L 2.5–4.2 earthquakes along the plate interface using waveform coda and find along-strike variations that mimic bathymetric variability. Median stress values are higher (3.2 MPa) in the smooth northern region, with lower values in the central (2.1 MPa) and southern (0.7 MPa) segments. Higher apparent stresses along a zone of little suspected subduction topography imply increased coupling or higher friction along the interface. These results agree with geodetic and other seismic studies that suggest variable plate coupling along the Nicoya Peninsula.

Components: 9200 words, 7 figures, 2 tables.

Keywords: apparent stress; coda wave; plate coupling; seamounts; subduction zone.

Index Terms: 7230 Seismology: Seismicity and tectonics (1207, 1217, 1240, 1242); 7240 Seismology: Subduction zones (1207, 1219, 1240).

Received 10 February 2011; **Revised** 23 May 2011; **Accepted** 31 May 2011; **Published** 4 August 2011.

Stankova-Pursley, J., S. L. Bilek, W. S. Phillips, and A. V. Newman (2011), Along-strike variations of earthquake apparent stress at the Nicoya Peninsula, Costa Rica, subduction zone, *Geochem. Geophys. Geosyst.*, *12*, Q08002, doi:10.1029/2011GC003558.

1. Introduction

[2] Understanding the role of fault zone conditions on resulting earthquake rupture is an important component of earthquake studies, but one that is difficult to address due to poor constraints on both conditions of the fault and earthquake source parameters. This link between rupture and fault condition is important for all fault environments, with irregularities and fault roughness noted on faults around the world. Within subduction zones, a wide range of features can exist to modify the plate interface fault contact, such as variable sediment

thickness, plate bending related faults, and topography associated with transforms, seamounts, and ridges. All have been related in some way to variations in plate interface seismicity, from controlling the size of rupture to influencing the rupture propagation of large earthquakes [e.g., *Ruff*, 1989; *Ryan and Scholl*, 1993; *Bürgmann et al.*, 2005; *Bangs et al.*, 2006; *Robinson et al.*, 2006].

[3] In one model, subducting topography, such as seamounts, creates large asperities that increase the normal stress on the interface, thus increasing the coupling strength at that point on a fault [*Cloos*, 1992; *Scholz and Small*, 1997; *Scholz*, 2002]. Alternatively, recent work suggests that seamounts at shallow depths within the subduction channel may weaken plate coupling through release of fluids [*Mochizuki et al.*, 2008]. However, this model of weak plate coupling at seamounts may be valid for the features at the shallowest depths where fluids are abundant. As fluid availability decreases to near 10% of original volume, normal stress and thus interface coupling will increase at the seamount [*von Huene*, 2008]. In areas of little subducted topography the interface is smoother and hence contact is expected to be continuous and pervasive. This smooth contact may lead to either strong or weak interface coupling depending on the content and thickness of relatively weak sediment.

[4] These complex interactions between subducting plate conditions and coupling strength will also impact the nature of earthquakes occurring along the plate interface. Various studies, relying on the model of strong coupling at topographic plate features, have linked specific geologic features such as seamounts to areas of high slip during individual earthquakes [e.g., *Protti et al.*, 1995; *Abercrombie et al.*, 2001; *Husen et al.*, 2002; *Bilek et al.*, 2003a]. These studies focus primarily on large magnitude earthquakes because global recording of these events makes it possible to study the rupture characteristics. However, large events are relatively infrequent during the period of instrumentation, thus it is difficult to explore regional along-strike variations using only such large events. Analysis of more frequent, smaller magnitude events provides increased sampling along the subduction margin.

[5] Here we focus on the northwestern Costa Rica subduction zone in Central America where previous onshore-offshore seismic networks captured thousands of earthquakes in a region of significant along-strike variation of geologic parameters. Local recording of earthquakes by the Costa Rica Seismogenic Zone Experiment (CRSEIZE) from 1999 to 2001 produced a high-quality data set that allows us to determine earthquake source parameters for comparison with the geologic variability produced by the two distinct origins of the subducting Cocos Plate (Figure 1). Thus our goal is to determine the effects of the subducting topography on earthquake rupture process in the Cocos-Caribbean Plate convergent margin by computing apparent stress (σ_a) using earthquake coda spectral amplitudes. The Costa Rican convergent margin is ideal for this study because the Nicoya Peninsula lies directly above the seismogenic zone, making local recording of smaller magnitude events possible. Additionally, the subducting Cocos Plate has origins at both the East Pacific Rise (EPR) and Cocos-Nazca (CNS) spreading centers, a junction that manifests itself in different topographic features on either side.

[6] We focus on the earthquake source parameter apparent stress to compare with subducting plate variations because of its previous use in global studies, and its calculation stability. Apparent stress (σ_a), a measure of stress drop combined with seismic efficiency [*Wyss and Molnar*, 1972; *McGarr*, 1999], has been used in numerous studies to evaluate source properties [e.g., *Mayeda et al.*, 2003; *Eken et al.*, 2004; *Prieto et al.*, 2004; *Choy and Kirby*, 2004; *Malagnini et al.*, 2006; *Choy et al.*, 2006; *Mayeda and Malagnini*, 2009]. Average σ_a varies with faulting mechanism, tectonic and regional setting [*Choy and Boatwright*, 1995], and it can reflect the maturity of the rupturing fault [*Choy et al.*, 2006]. Earthquakes with high average σ_a tend to occur in intraplate portions of oceanic slabs, near spreading ridges and transform faults, where young, immature faults rupture. In contrast, earthquakes along the subduction interface tend to have low average σ_a [*Choy and Boatwright*, 1995; *Choy et al.*, 2006]. *Choy and Boatwright* [1995] suggest that irregularities on the fault surface may cause locally increased σ_a due to resulting changes in local stress conditions.

[7] In this study, coda wave amplitudes are used to calculate σ_a (Figure 2), because of their demonstrated stability over body wave amplitude measurements [e.g., *Mayeda*, 1993]. Coda waves originate as body and surface waves that scatter in the Earth due to inhomogeneities along the path from their source to the recording station [*Aki*, 1969; *Aki and Chouet*, 1975]. The increased stability of coda amplitude–derived apparent stress calculations comes from the averaging power of scattered waves, thus making results less dependent on source radiation patterns and crustal heterogeneities [*Chouet et al.*, 1978; *Rautian and Khalturin*, 1978; *Mayeda*, 1993; *Mayeda and Walter*, 1996; *Eken et al.*, 2004;

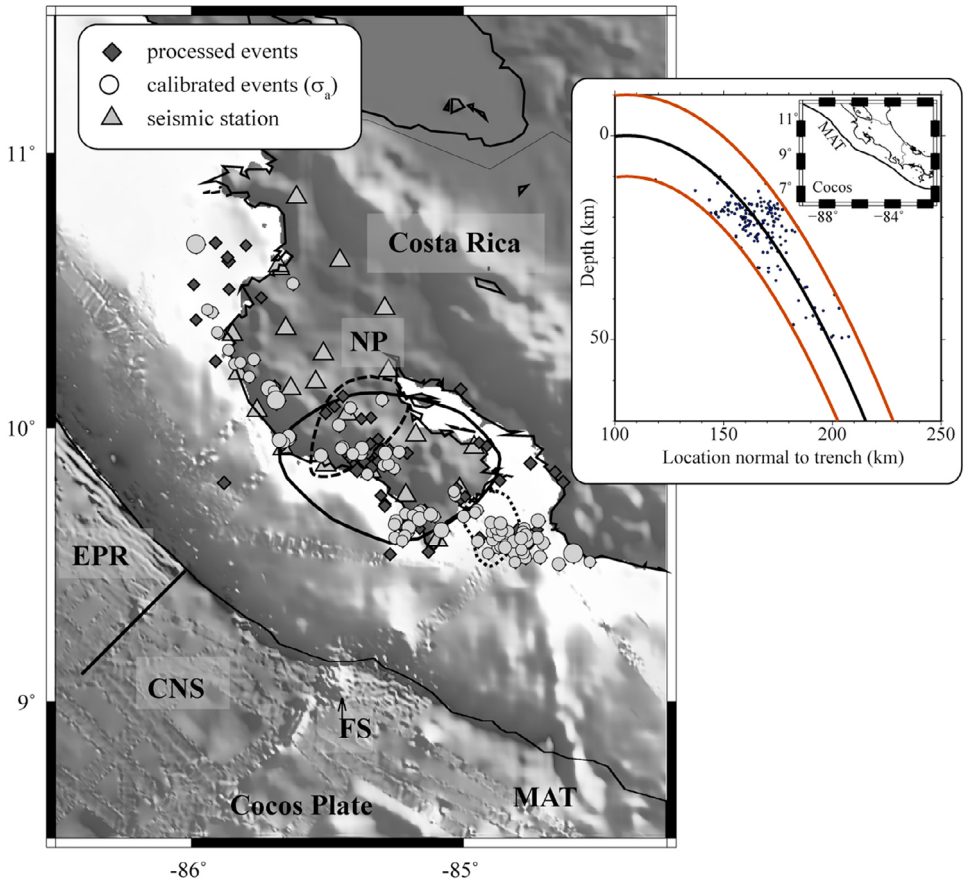

Figure 1. High-resolution physiographic image of the study area, including the subducting Cocos Plate near Nicoya Peninsula (NP), Costa Rica [*Ranero et al.*, 2003; ETOPO2v2 Global Gridded 2-minute Database, National Geophysical Data Center, National Oceanic and Atmospheric Administration, U.S. Department of Commerce, http://www.ngdc.noaa.gov/mgg/global/etopo2.html] showing earthquakes used in this study. The Cocos Plate subducting along the northern portion of Nicoya is relatively flat (crust originated at East Pacific Rise (EPR)). At the southern boundary of the peninsula, the portion of Cocos Plate that originates at the Cocos-Nazca spreading center (CNS) carries seamounts and ridges into the trench. The suture between the two structurally distinct portions of the plate shows in the bathymetry data as vertically offset seafloor (solid line). The Fisher seamount (FS) and ridge are subducting at the southern tip of the Nicoya Peninsula. All 161 processed earthquakes are shown as black diamonds. Out of the 161, 94 were well calibrated and used to compute apparent stress (white circles). Station locations are shown as gray triangles. Also shown are rupture areas for the 1950 (solid line), 1978 (dashed line), and 1990 (dotted line) earthquakes at the Nicoya Peninsula and a cross section of the processed events (orange lines represent ±10 km distance from the interface).

Malagnini et al., 2004, 2006; *Mayeda et al.*, 2007]. The interstation coda amplitude measurements tend to be very similar over a range of seismic network size and tectonic setting, which makes this technique ideal for spectral studies in regions with sparse network coverage, large tectonic complexity, or unknown subsurface structure [e.g., *Eken et al.*, 2004; *Malagnini et al.*, 2004].

2. Tectonic Setting

[8] Nicoya Peninsula, Costa Rica, is situated above the seismogenic zone resulting from the convergence between the Caribbean and Cocos plates (Figure 1). The Pacific, Cocos and Nazca plate triple junction system moves northward, although the boundary has undergone several ridge jumps toward the south, possibly due to the Galapagos plume position [*Hey*, 1977; *Barckhausen et al.*, 2001]. New Cocos Plate crust is formed at the CNS in the south, and at the EPR in the west. The suture is manifested by a narrow ridge that subducts beneath the central Nicoya Peninsula [*von Huene et al.*, 2000; *Barckhausen et al.*, 2001; *Fisher et al.*, 2003].

[9] The variable origin of the Cocos Plate affects its structural character. There are differences across

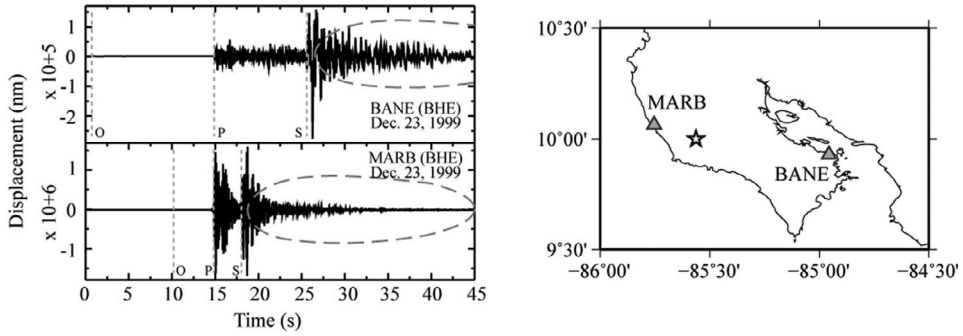

Figure 2. (left) Example earthquake waveforms recorded on the Nicoya Peninsula for an M_L 4.1 earthquake (star in Figure 2 (right)) that occurred on 23 December 1999 (00:36:05 UTC) recorded at stations BANE and MARB (triangles in Figure 2 (right)). This event occurred very close to MARB. The body wave arrivals (*P* and *S*), origin times (O), and coda wave energy (dashed gray circles) are shown for both stations. (right) Locations of stations and earthquake.

the EPR-CNS suture in the temperature of the plate entering the trench, its topography, seismogenic updip limit, and the geologic structures in the fore arc [*Fisher et al.*, 1998; *Silver et al.*, 2000; *von Huene et al.*, 2000; *Harris and Wang*, 2002; *Newman et al.*, 2002; *Fisher et al.*, 2003; *Spinelli et al.*, 2006; *Sak et al.*, 2009, *Harris et al.*, 2010a, 2010b]. All of these variations may impact seismicity and deformation, so we review current understanding of these parameters here.

2.1. Thermal State of the Cocos Plate

[10] It is thought that the EPR origin crust is colder than the CNS origin crust due to higher hydrothermal circulation. The crustal age varies from about 19 Myr at the southern edge of the Peninsula to 24 Myr along the northern Nicoya Peninsula, with about 1.5 Myr jump at the suture [*Barckhausen et al.*, 2001]. The conductive heat flow within the EPR crust is low, only 20–40 mW/m^2, which is attributed to high permeability of the oceanic basement rock formed at the faster spreading EPR [*Fisher et al.*, 2003]. High permeability, and consequently low conductive heat flow, for crust formed at the EPR is also suggested by *Silver et al.* [2000], who estimate conductive heat flow values north of the EPR-CNS suture to be only about 10% of that expected for 24 Ma old oceanic crust. The heat flow of CNS origin crust is 105–115 mW/m^2, consistent with conductive lithospheric models [*Fisher et al.*, 2003]. *Harris et al.* [2010a] find similar patterns of low heat flow along the EPR and high heat flow in the CNS region, with a sharp transition along the suture.

[11] This variable plate temperature affects the updip limit of the seismogenic zone across the EPR-CNS suture. *Harris and Wang* [2002] modeled the thermal conditions of subducting EPR crust beneath northern Nicoya Peninsula to estimate the seismogenic updip limit as given by the intersection of 100°C and the onset of seismicity. Their results show that the 100°C isotherm for EPR crust is about 60 km landward from trench, and approximately 50 km from the trench for CNS crust [*Harris and Wang*, 2002; *Spinelli and Saffer*, 2004; *Spinelli et al.*, 2006]. These temperature variations may also be linked to variations in fluid pressure, with lower fluid pressure in the colder EPR crust, thus impacting the stress needed for seismogenesis [*Spinelli et al.*, 2006]. Models incorporating more recent heat flow measurements also show an along-strike difference in plate boundary temperatures, particularly in the upper 30 km [*Harris et al.*, 2010b].

2.2. Seismicity Distribution

[12] Several large historic earthquakes have been observed along the subduction megathrust within the Nicoya Peninsula region. Large earthquakes with magnitude ≥7.0 were identified along this region in 1900, 1916, 1939, 1950, 1978, and 1990 [e.g., *Nishenko*, 1991]. Most of these do not have strong constraints on the rupture areas, although estimates suggest similar epicenters for 1900 and 1916 [*Tristan*, 1916]. The 5 October 1950 moment magnitude (M_w) 7.7 earthquake located within central Nicoya Peninsula caused liquefaction, landslides, and a sudden drop in sea level. Sea level rise along the peninsula since 1950 suggests that the plate interface in the central region of Nicoya Peninsula is locked as the peninsula subsides during this interseismic period [*Güendel et al.*, 1989; *Marshall and Anderson*, 1995]. On 23 August 1978, a surface wave magnitude (M_S) 7.0 earthquake occurred near the 1950 earthquake, also likely on the plate interface [*Marshall and Anderson*, 1995;

Avants et al., 2001]. On 25 March 1990, an M_w 7.0 earthquake occurred at the entrance to the Gulf of Nicoya [*Protti et al.*, 1995], likely associated with fracturing of or near a previously subducted seamount [*Husen et al.*, 2002; *Bilek et al.*, 2003a]. However, this event did not rerupture the 1950 zone, making this entire peninsula a region classified as a seismic gap [*Nishenko*, 1991; *Protti et al.*, 1995]. The rupture areas for these three events are shown in Figure 1 with solid line for the 1950 event, dashed line for the 1978 event, and dotted line for the 1990 event.

2.3. Topography and Bathymetry

[13] Bathymetry changes vary along the Cocos Plate offshore Nicoya, as the plate is smooth where it subducts beneath the northern portion of the Nicoya Peninsula and it contains several seamounts near the southern tip of the peninsula, reflective of the difference in plate origin (Figure 1). South of the EPR-CNS suture, the trench slope is indented and rough in response to the subduction of seamounts [*Hinz et al.*, 1996; *Scholz and Small*, 1997; *Dominguez et al.*, 2000; *von Huene*, 2008]. The Costa Rica fore arc deforms in response to the subduction of these features [*Ye et al.*, 1996; *Gardner et al.*, 2001], which may range in height from 2 to 2.5 km [*Ranero and von Huene*, 2000].

2.4. Deformation

[14] Geodetic data collected in Costa Rica show continuous deformation that is characteristic of an interseismic cycle in a subduction zone, where the southern shorelines of Nicoya Peninsula are subsiding and uplift occurs in the interior [*Lundgren et al.*, 1999; *Norabuena et al.*, 2004; *LaFemina et al.*, 2009]. These studies suggest a locked patch near the central part of the Nicoya Peninsula, approximately in the area where the EPR-CNS suture is subducting, as well as a locked patch beneath the northern Nicoya Peninsula. Transient slip has been observed at the eastern tip of the Nicoya Peninsula at 25–30 km depth [*Outerbridge et al.*, 2010].

3. Data

[15] The seismic waveform data for this project were collected using a temporary seismic network deployed around Nicoya Peninsula as a part of the 1999–2001 CRSEIZE project. Twenty short-period and broadband land seismometers recorded for 18 months (December 1999 to June 2001), and were augmented by 14 ocean bottom seismometers during the first six months. The network recorded approximately 10,000 small magnitude ($M_L < 6.4$) earthquakes in the region [*Newman et al.*, 2002; *DeShon et al.*, 2006, *Ghosh et al.*, 2008], encompassing interplate events as well as intraslab and upper plate events. The most complete catalog to date comes from *Ghosh et al.* [2008], which is found to be complete along the Nicoya interface for events with $M_L \geq 2.4$ with mean formal location errors of approximately 1.5 km horizontal and 2.7 km in depth for events in the proximity to the Nicoya Peninsula. Selected earthquakes from this data set that occurred along the subduction zone interface were used to describe the seismogenic updip limit variation across the EPR-CNS suture [*Newman et al.*, 2002], to determine focal mechanisms [*Hansen et al.*, 2006], and map the *b* value distribution along strike and downdip of the trench [*Ghosh et al.*, 2008]. Out of our selected interface events, with the exception of one cluster of strike-slip earthquakes, the focal mechanisms for 14 individual and clustered events represent underthrusting faulting along the interface [*Hansen et al.*, 2006]. Thus we do not compute mechanisms for our individual events, assuming that seismicity is dominated by plate interface activity.

[16] Because the peninsula is close to the trench, the CRSEIZE instruments provided high-quality data focused at the interface between the Cocos and the Caribbean plates. The data selected for this study consists of 161 events that located between 9.5° and 11°N and 86° and 84.5°W, within 10 km of the subducting plate interface, and up to a depth of 50 km. The 50 km depth cutoff is used to constrain the data to the locked part of the subduction zone interface. Results here are based solely on land-based seismometer data due to better signal-to-noise ratio (SNR). These seismometers sampled at 20 or 40 Hz, which constrained the usable frequency range of the earthquake signal processing.

[17] Event-based waveforms are windowed to contain 20 s before the *P* wave and 180 s following *P*. The earthquake signal varies in quality due to the event size and distance from the network or individual station, but it is generally of high quality such that the *P* and *S* phase arrivals and coda energy are clearly visible (Figure 2).

4. Methods

[18] Using earthquake coda amplitudes instead of body wave amplitudes provides more stable amplitude measurements due to the averaging properties of

Table 1. Frequency-Dependent Calibration Parameters[a]

f (Hz)	swide (s)	delint (s)	t_{start} (s)	t_{max} (s)	t_{meas} (s)
0.5–0.7	10.0	3.0	20.0	20.0	33.0
0.7–1.0	8.0	3.0	12.0	20.0	25.0
1.0–1.5	6.0	2.0	10.0	25.0	27.0
1.5–2.0	6.0	2.0	5.0	30.0	25.0
2.0–3.0	4.0	1.0	5.0	30.0	25.0
3.0–4.0	3.0	1.0	5.0	30.0	25.0
4.0–6.0	3.0	1.0	5.0	30.0	25.0
6.0–8.0	3.0	1.0	5.0	25.0	22.0
8.0–10.0	3.0	1.0	5.0	20.0	28.0
10.0–13.0	3.0	1.0	5.0	20.0	18.0
13.0–16.0	3.0	1.0	5.0	20.0	18.0
16.0–19.0	4.0	1.0	5.0	25.0	22.0

[a]From the original Mayeda bands [e.g., *Eken et al.*, 2004] we added bands above 2 Hz in order to constrain ω_c and amplitude decay at higher frequencies. Shown here are the smoothing width (swide) and interpolation interval (delint) and coda window start time (t_{start}), maximum duration time (t_{max}), and coda measurement time (t_{meas}) for each frequency band with respect to maximum coda peak amplitude.

coda over path and radiation effects [e.g., *Aki*, 1969, *Aki and Chouet*, 1975, *Chouet et al.*, 1978; *Rautian and Khalturin*, 1978; *Phillips and Aki*, 1986; *Eken et al.*, 2004; *Malagnini et al.*, 2004; *Mayeda et al.*, 2005; *Malagnini et al.*, 2006]. This method is ideal for the Nicoya Peninsula setting because small numbers of stations recorded each event. The data processing and initial analysis follows the method of *Mayeda et al.* [2003] and *Phillips et al.* [2008], followed by application of a spectral ratio method to obtain source amplitudes. More details regarding the methods are found in the auxiliary material.[1]

4.1. Narrow-Band Envelopes

[19] Because the behavior of earthquake coda is strongly frequency dependent due to source effects and changes in anelastic processes and/or crustal structure [*Mayeda and Walter*, 1996], the original seismic record for each earthquake and station pair is divided into narrow-band, roughly half-octave, frequency envelopes. The envelopes for each frequency band are formed as a sum of the instrument-corrected, filtered velocity seismogram and its Hilbert transform [*Mayeda et al.*, 2003]. Then, horizontal component envelopes are stacked and averaged. The frequency range of each band, corresponding smoothing width, and final interpolation interval are given in Table 1.

[1]Auxiliary materials are available in the HTML. doi:10.1029/2011GC003558.

4.2. Coda Windows

[20] We used S and Lg coda in this study. Coda endpoints were chosen manually at the bottom of a slope of steepest decaying amplitude, yet above the background noise level. We use offset relative to the peak envelope (t_{start}), and coda maximum duration (t_{max}, Table 1) parameters to set the coda windows. The coda window spans over the time domain bounded by t_{start} and t_{max}. The t_{start} is set with respect to coda peak for all bands (Table 1). The t_{max} is larger for lower-frequency bands, and the coda amplitude will be measured at t_{meas}, generally within 5–15 s of t_{max}.

4.3. Initial Coda Calibration

[21] We start by calibrating coda shape and path behavior for the Nicoya region. This allowed for minor distance related adjustments prior to taking coda ratios. *Phillips et al.* [2008] express the coda amplitude (A) as

$$A_{ij}(f) = S_i(f)T(\varphi_i,\theta_i,f)P'\left(\varphi_i,\theta_i,\varphi_j,\theta_j,f\right) \cdot R'_j(f)D'_j[x,f,t_c(x,f)+t_{meas}(f)], \quad (1)$$

where f is frequency, x is distance, i and j are source and receiver indices, φ is latitude, θ is longitude, t_c is coda origin time calibrated to coincide with the peak envelope, and t_{meas} is the time at which we measure coda amplitude. S is the source amplitude spectra, T is the source-to-coda transfer function, P' represents path effects, R' is the site term, and D' represents the coda decay function. The primed factors represent dimensionless terms. In this study we compute the coda origin, t_c, shape functions, D', and path effects, P', as functions of frequency.

[22] The corrections to coda amplitude are done in several steps. First, automatically determined coda peak times are used to calibrate the coda peak group velocity (v_g), thus coda origin time. The coda v_g is estimated following *Mayeda et al.* [2003] as a hyperbolic distance-dependent function fit to the coda peak times for every frequency band. The fitting is performed using the Powell direct search method [*Press et al.*, 2007], based on an L1 norm minimization criterion. As the stations in our network are closely spaced, we group them together to estimate the peak v_g for the region. The t_c and v_g are used to compute the coda shape functions, D' in a similar manner, again using hyperbolic functions of distance [*Mayeda et al.*, 2003], based on windowed coda data. After fitting the shape function to an individual envelope, we interpolate the coda

Table 2. Seismic Moments Computed Using Waveform Inversion Compared to Coda Moments[a]

Event ID	M_{0w} (log Nm)	M_{0c} (log Nm)	ω_c (Hz)	M_L	Depth (km)
2963	15.24	15.13	4.09	4.11	21
23018	13.89	13.83	6.16	3.10	16
25897	14.52	14.47	5.59	3.46	19

[a]M_{0w} denotes waveform inversion [*Bilek et al.*, 2003b], and M_{0c} denotes coda moments. Table 2 also includes corner frequencies (ω_c obtained using coda calibration), original magnitudes (M_L), and depths.

amplitudes at time t_{meas} given for each frequency in Table 1.

[23] We perform quality control of the coda amplitudes by comparing the original earthquake magnitude, M_L [*Ghosh et al.*, 2008], after correcting from a magnitude-based scaling model [*Taylor and Hartse*, 1998], removing obvious outliers. The *Taylor and Hartse* [1998] model uses the original magnitudes to estimate propagation effects on coda amplitude. Then we invert for site effects and one-dimensional attenuation (quality factor Q) for each band based on relative amplitudes for each event using an L1 Powell method (terms P' and R', equation (1)). We also solve for laterally varying Q [*Phillips et al.*, 2008], finding that a single Q is sufficient for this small region. The initial Q estimate corresponds roughly to the value of Q at 11 Hz using coda Q results from *Gonzalez and Persson* [1997] for the Nicoya Peninsula.

[24] We obtain the coda source amplitudes using a technique based on coda amplitude spectral ratios [e.g., *Mayeda et al.*, 2007], with extensions for use with large data sets [*Phillips et al.*, 2010]. Amplitude ratios were calculated by directly comparing codas for event pairs within 20 km of each other, and stacking results for different stations. Calibration parameters for coda origin, shape and path were applied at this time to account for small distance differences. The event pair amplitudes were then inverted to obtain event amplitudes relative to their mean in each band. These amplitudes were used to solve for seismic moment, M_o, corner frequency, ω_c, and transfer function terms using the Brune source model [*Brune*, 1970]. Absolute levels are obtained by constraining moments to independently determined values based on waveform inversion [*Bilek et al.*, 2003b] for three events in our data set (Table 2). Using results for M_o and ω_c, we solve for apparent stress, σ_a, following *Walter and Taylor* [2001]:

$$\sigma_a = \omega_c^3 M_o / K, \tag{2}$$

where the factor K is computed as

$$K = 16\pi/\left(\beta^2\left(R^2_{\theta\Phi P}\xi^3/\alpha^5 + R^2_{\theta\Phi S}/\beta^5\right)\right), \tag{3}$$

where β and α are the source area S and P wave velocities for the region taken from *DeShon et al.* [2006], $R_{\theta\Phi S(P)}$ are average S and P wave source radiation terms (0.44 and 0.6, respectively) [*Walter et al.*, 2007], and ξ is the ratio of P and S wave corner frequencies (set to 1).

[25] The model fits the corrected amplitude spectrum of the events with independent M_0 estimate well, with final model RMS 0.07 and variance 0.006 (Figure 3). Out of the 161 processed earthquakes, 94 had well-constrained corner frequencies and were used in the interpretation of the apparent stress variation within the Nicoya Peninsula subduction zone.

5. Results

[26] Using the coda amplitude spectral ratio method, well-constrained source spectra for earthquakes located at the plate interface can be obtained, and hence variations in source parameters along strike and downdip are identifiable. The ω_c and spectral fit quality control requirements are to have at least one calibrated frequency band above and below ω_c. For the events with independent M_0 estimates, we compute RMS and variance for the model fits to the spectra, finding very good fits (RMS 0.07 MPa, variance of 0.006) to the spectra. We also tested varying the seismic velocities and radiation patterns by ±5%, which in turn changes the K variable in equation (2) by about 5%. This resulted in maximum σ_a RMS difference of 0.5 MPa, with majority of events having <0.1 MPa difference. Based on these quality control requirements and tests, our final data set of 94 earthquakes has well-constrained spectra and source parameters.

5.1. Scaling Model

[27] In the *Brune* [1970] source model, M_o is proportional to ω_c^{-3} over a range of earthquake magnitudes although this model of cube root proportionality may not be valid for all magnitudes. For example, *Kanamori and Rivera* [2004] find that the radiated energy (E_r) to moment ratio, (E_r/M_o) a parameter commonly used to estimate apparent stress, increases with magnitude, thus implying that the cube root proportionality between M_o and ω_c does not hold for all event sizes. Other studies show this ratio as

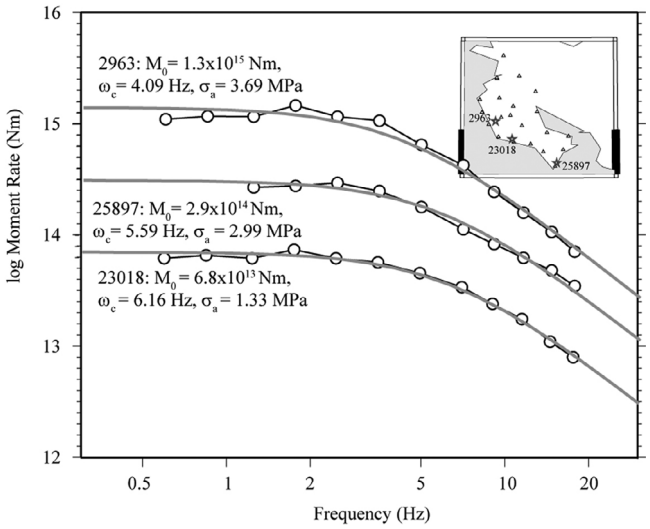

Figure 3. Source spectra model (gray line) of earthquakes with M_0 estimated using waveform inversion after applying transfer function to the path and source corrected amplitudes (open circles). Inset shows event location (stars) and station distribution (triangles).

constant however [e.g., *Choy and Boatwright*, 1995; *Newman and Okal*, 1998]. *Kanamori and Rivera* [2004] show that if the cube root is modified by a positive constant (η, which is ≤ 1), so that M_o is proportional to $\omega_c^{-(3+\eta)}$, the fit between the observed source parameters and their modeled relationship improves significantly. Similarly, *Walter and Taylor* [2001] and *Mayeda et al.* [2003] allow for variable scaling of M_o with ω_c (allowing $\eta > 0$) computed using coda wave amplitudes, and show that the calibrated source spectra fit such a model better. Therefore, this study follows the method of *Mayeda et al.* [2003] allowing for variable scaling.

5.2. Along-Strike Apparent Stress Variation

[28] The geometric mean earthquake σ_a for the entire Nicoya data set is 1.3 MPa, the median is 1.2 MPa. We find along-strike variations in the subduction zone, with smaller values along the southern portion and higher values along the northern portion of the peninsula (Figure 4). In general, the σ_a values are mostly below 1.0 MPa at the southern end, below 2.0 MPa at in the central part, and above 2.0 MPa along the northern portion of the peninsula. Earthquake with the largest σ_a (12.3 MPa) located in the east part of the Gulf of Nicoya. The highest σ_a values for each region were 12.3 MPa in the southern, 10.1 MPa near the central part, 9.2 MPa in the northern portion of the Nicoya Peninsula. Standard deviations are 1.9 MPa in the northern segment, 2.7 MPa in the central segment, and 1.7 MPa in the southern segment. Six earthquakes with the lowest σ_a values (<0.3 MPa) occurred all near the southern portion of the Nicoya Peninsula.

[29] Across the EPR-CNS suture there is a significant difference in σ_a, with a median σ_a of 3.3 MPa (geometric mean 3.6 MPa) on the EPR side and 1.0 MPa (geometric mean 1.0 MPa) on the CNS side. The smallest median values (0.7 MPa) from 54 calibrated events are located at the southern tip of the peninsula (block A, Figure 4). Within this group, only the highest σ_a event (12.1 MPa) is located deeper at about 35 km, the others are located between 13 and 30 km. In the central portion of the peninsula, the median σ_a transitions to higher values (2.1 MPa) using 19 well-calibrated events (block B, Figure 4). At the northern end of the peninsula, the median σ_a values (3.2 MPa) are significantly larger than those observed in the south, based on 13 well-calibrated earthquakes (block C, Figure 4). Out of the 19 highest σ_a earthquakes in these regions ($\sigma_a >$ 3.0 MPa), there are 9 events (47%) located near the central block, 8 events (42%) in the north block, and 2 (11%) events located near the southern block.

5.3. The σ_a Variation With Depth

[30] Several 5 km wide depth bins were used to compare the median σ_a variation across the EPR-CNS suture (Figure 5). There were no calibrated earthquakes shallower than 15 km on the EPR crust. For the depth range 15–50 km, the EPR has consistently higher median σ_a compared to the CNS. Thus the variation in coupling across the EPR-CNS

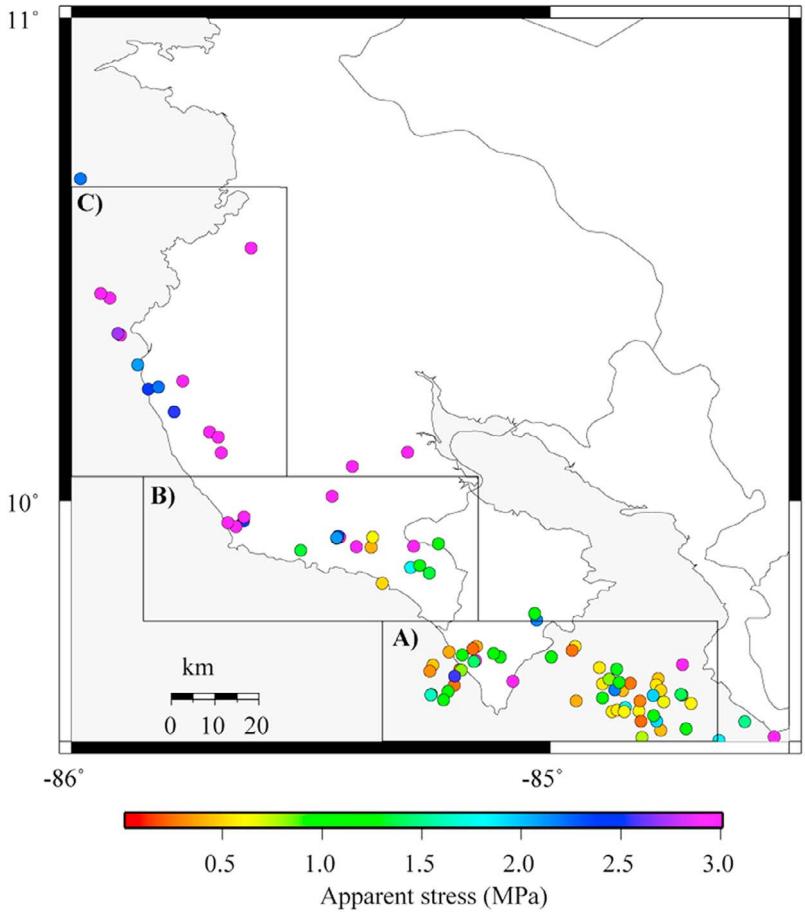

Figure 4. Apparent stress (σ_a) distribution for 94 well-constrained events. The colors span σ_a range between 0.1 and 3.0 MPa; earthquakes with σ_a above 3.0 MPa (ranging up to 12.3 MPa) are shown as purple circles.

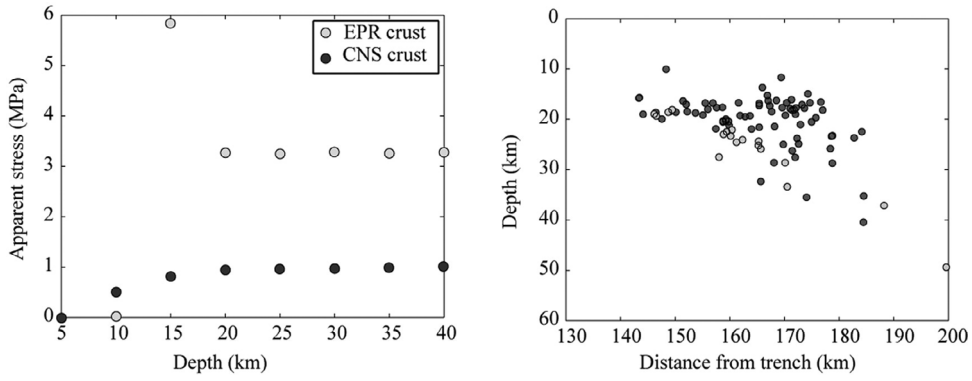

Figure 5. (left) Median σ_a variation across the EPR-CNS suture for 5 km wide depth bins. (right) Cross-sectional view along strike of the MAT along EPR (light circles) and CNS (dark circles) crust events.

suture that persists at all depth intervals reflects the physical differences of the subducting plate.

6. Discussion

6.1. Global Comparisons

[31] Our geometric mean estimates of the apparent stress along the Nicoya Peninsula are 1.3 MPa, which is higher than the apparent stress observed for globally averaged subduction zone earthquake data sets. *Choy and Boatwright* [1995] and *Choy et al.* [2006] determined a global average σ_a of 0.29 MPa for thrust earthquakes occurring within subduction zones, and a regional average σ_a of 0.28 MPa for a subset of 8 events along the entire Middle America trench. Calculation methods do differ between the studies, as *Choy and Boatwright* [1995] compute apparent stress through determination of the radiated energy (E_r) moment ratio using body waves. *Allmann and Shearer* [2009] computed stress drop, another parameter than can be related to our apparent stress values, using *P* wave spectra for a global data set of earthquakes. Similar to the trend found by *Choy and Boatwright* [1995] and *Choy et al.* [2006], *Allmann and Shearer* [2009] found some of the lowest median stress drops for subduction zone earthquakes (2.98 MPa), relative to transform faults and intraplate events with much higher median stress drop (~6 MPa). *Allmann and Shearer* [2009] estimate is close to what we observed for the median σ_a on the EPR crust (3.3 MPa).

6.2. Along-Strike Variations

[32] *Choy and Boatwright* [1995] and *Choy et al.* [2006] relate variable σ_a observed in different tectonic settings to level of fault maturity and fault strength. Subduction zone megathrust events have the lowest σ_a in their studies, roughly a factor of ~20 lower than found for events that occurred on intraoceanic strike slip faults that break relatively new fractures. Thus they claim that the more mature, or higher cumulative displacement, subduction faults are generally lower strength faults and their earthquakes release less higher frequency energy, resulting in lower σ_a. The higher σ_a events occur on less mature, or less cumulative displacement, fault contacts that they infer to be stronger, thus producing more high frequency energy during rupture.

[33] We can apply these ideas to the along-strike variations that we observe along the Nicoya Peninsula. On average, events in northern portions of the Cocos Plate where EPR crust subducts have higher σ_a (geometric mean 3.6 MPa) than for events located along the southern segments where the CNS crust is subducted (geometric mean 1.0 MPa). This factor of > 3 difference in σ_a persists even when subdividing the region into smaller segments. Based on these differences, we infer a reduction in fault coupling strength as we move from north to south along the Nicoya Peninsula.

[34] This large change in apparent stress and inferred coupling is coincident with the change from EPR to CNS origin Cocos Plate. This junction also marks a change in Cocos Plate character, from smooth in the north to seamount laden in the south. One possibility is that this morphologic change leads to the change in coupling, with the smoother EPR origin plate allowing more continuous and stronger contacts to develop. To the south, the heterogeneous distribution of seamounts might disrupt contact areas and/or deform the overriding plate, producing weaker average coupling between the Cocos and Caribbean plates. At specific seamount–upper plate contacts, strong coupling might be possible, but on average the seamount region would be low coupling.

[35] There is also a change in heat flow and crustal temperature across this boundary, with the northern high σ_a area occurring on the colder EPR crustal contact. A possible connection between temperature, plate coupling, and σ_a may be related to fluid pressures. If the colder EPR portion has reduced fluid pressures [*Spinelli et al.*, 2006], this could increase normal stress and possibly lead to stronger plate coupling. These temperature differences may also affect various diagenetic reactions that could also cause the observed coupling variations.

[36] We can compare our results with estimates of past displacements, or fault maturity as defined by *Choy et al.* [2006], with large displacements indicating a higher degree of fault maturity than along segments with less displacement in past events. Rupture estimates for the M 7.7 1950 event encompass much of the southern portion of the peninsula where the low σ_a events are located (Figure 6). The northern extent of the 1950 rupture area, as well as an estimate of the rupture zone for the 1978 event, lie at the boundary between the EPR and CNS crust and within an area of high σ_a from our data set. The 1950 event is described as one of the largest events along the peninsula [e.g., *Protti et al.*, 1995]. Estimates for the 1900 and 1916 events suggest smaller magnitudes, M 7.2 and 7.4, respectively [*Nishenko*, 1991] and epicentral locations appear to be north of the northern tip of Nicoya Peninsula [*Tristan*, 1916; *Protti et al.*, 1995]. Based on these events,

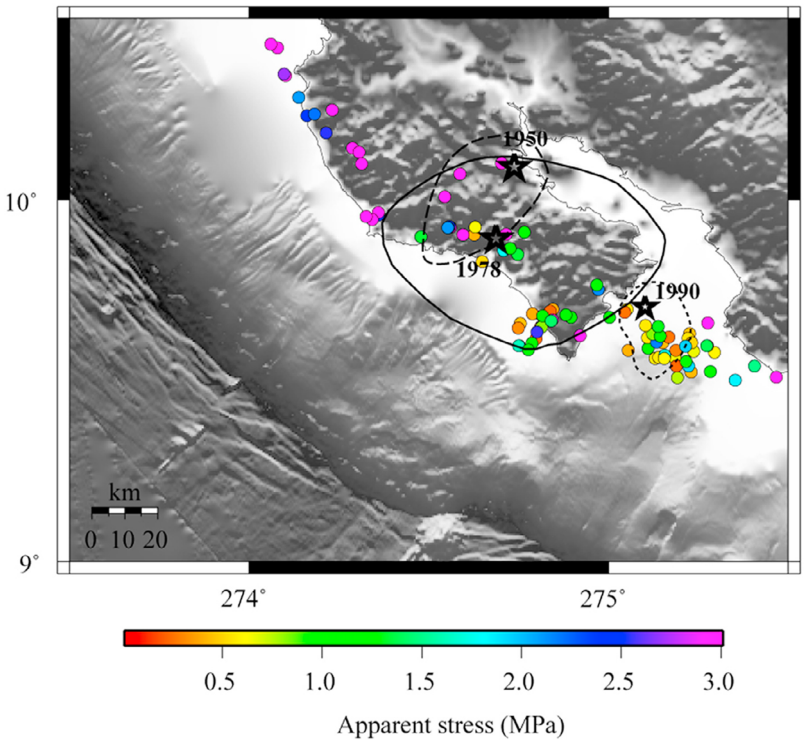

Figure 6. Apparent stress (σ_a) distribution for 94 well-constrained events. The colors span σ_a range between 0.1 and 3.0 MPa; earthquakes with σ_a above 3.0 MPa (ranging up to 12.3 MPa) are shown as purple circles. The median σ_a is 3.2 MPa at the northern portion of the peninsula (block C), 2.1 MPa at the central portion of the peninsula (block B), and 0.7 MPa at the southern portion of the peninsula (block A).

the southern portion of the peninsula may rupture in larger events than the northern portion, thus having more cumulative displacement and higher level of maturity. Based on the connections between σ_a and fault maturity proposed by *Choy and Boatwright* [1995] and *Choy et al.* [2006], our lower σ_a values are consistent with the higher degree of fault maturity in the south.

[37] We can also compare our apparent stress results to other measures of interplate fault coupling strength based on geodetic measurements along the Nicoya Peninsula. Both *Norabuena et al.* [2004] and *LaFemina et al.* [2009] used geodetic data collected at stations along the Nicoya Peninsula and inland Costa Rica to estimate the coupling along the plate interface. Here we compare our results to *LaFemina et al.* [2009] because of their use of additional years and stations in the solution, but in both models, the general pattern included a moderately locked patch in the northern portion of the Nicoya Peninsula with weaker coupling to the south (Figure 7). Our region of higher σ_a along the northern portion of the peninsula corresponds to the *LaFemina et al.* [2009] patch of 50% interface locking from their model 3. The southern portion of the peninsula maintains somewhat weaker coupling (locking values of 10–15%) in the regions of our lower average σ_a events. Thus our σ_a results are consistent with these geodetic results that indicate along-strike variations in plate coupling.

[38] Our estimates are also comparable to interface locking estimates based on seismic *b* value (relative frequency of small to large magnitude earthquakes) calculations by *Ghosh et al.* [2008]. Variations in *b* value within particular fault zones have been linked to possible fault coupling variations, with low *b* values in regions of high fault coupling or stress [e.g., *Schorlemmer and Wiemer*, 2005]. Spatial variations of well resolved *b* value determined along Nicoya using a much larger subset of the CR-SEIZE earthquake catalog indicate high *b* value (low coupling) in the south and low *b* values (high coupling) in the central portion of the peninsula [*Ghosh et al.*, 2008], consistent with our results of increasing median σ_a northward along the peninsula.

6.3. Role of Seamounts

[39] There are a few events in our data set that occur in the region of the 1990 M_w = 7.0 Nicoya

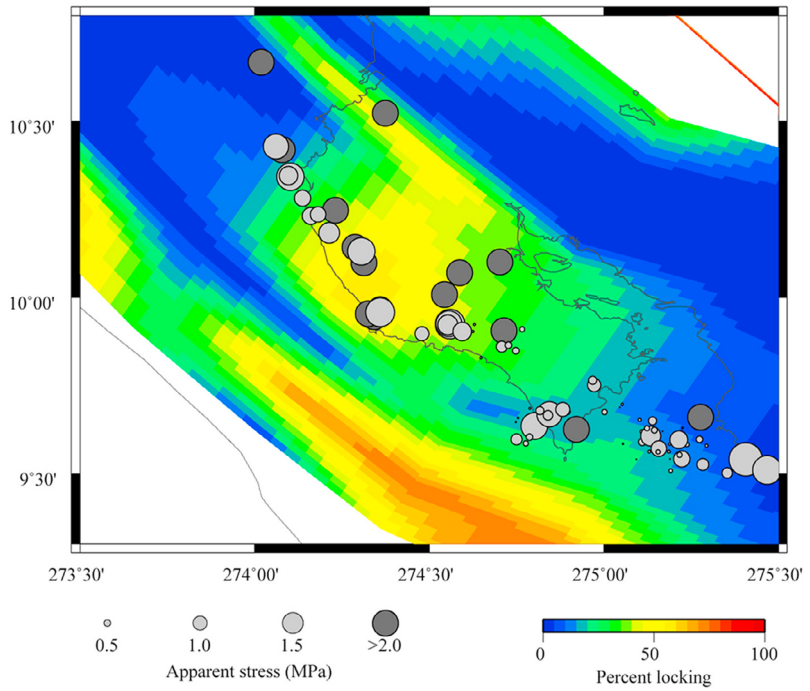

Figure 7. Geodetic locking on the subduction zone interface using CR-SEIZE GPS data (model 3 from *LaFemina et al.* [2009]) compared to the σ_a distribution (circles). The light gray circles represent average σ_a values below 2.0 MPa. The dark gray circles are of constant size and represent events with σ_a above 2.0 MPa (ranges up to 12.3 MPa).

Gulf earthquake, an event that has been related to rupture of a previously subducted seamount contact. Various models suggest that regions of subducted seamounts are areas of strong coupling [e.g., *Cloos*, 1992; *Scholz and Small*, 1997; *Scholz*, 2002] or alternatively areas of weak coupling [e.g., *Mochizuki et al.*, 2008]. Examination of σ_a within this portion shows median 0.6 MPa, which is about the same as the rest of the southernmost segment A (median 0.7 MPa, Figure 4). However, the event with σ_a 12.3 MPa (depth 35 km) found in the southern segment occurred just east of this area. Thus, we suggest that these Nicoya Gulf events provide support for the idea that subducted seamounts are areas of high fault strength, leading to higher σ_a events.

[40] *Mochizuki et al.* [2008] note depth dependence in coupling relative to seamount position within the Japan Trench, with low coupling directly over the seamount and higher coupling downdip. For the seamount proposed in the Nicoya Gulf region, depth estimates of this feature range from 20 to 30 km based on tomography studies [*Husen et al.*, 2002, 2003] and 20 km based on waveform inversion of the 1990 earthquake [*Protti et al.*, 1995]. *Husen et al.* [2003] also relocate seismicity recorded by local, on-land permanent networks between 1984 and 1997, and find a dense cluster of events within and directly above the low-velocity feature they identify as the subducted seamount, also suggestive of high coupling at the seamount–upper plate contact. The high σ_a event in our data set that occurred just east of the 1990 rupture area located at 35 km depth, suggesting that it might be near the downdip contact of the subducted seamount.

6.4. Depth Variations

[41] At greater depth along the subduction zone interface, the normal stresses acting on the interface increase, sediment compaction occurs, and the amount of fluids decreases, which can result in higher coupling strength along the interface. One might expect an increase in σ_a with depth due to the increased strengthening of the materials at the plate contact. There is no suggestion of such increase on either EPR or CNS crust, as after 15 km depth the median values up to 40 km remain relatively constant (Figure 5).

7. Conclusions

[42] We compute apparent stress for 94 earthquakes located along the plate interface on the western

Costa Rica margin, focused on the Nicoya Peninsula. We find geometric average σ_a values are higher than global averages for subduction zones, and along-strike trends that suggest increased plate coupling (higher σ_a) along the northern portion of the Nicoya Peninsula where EPR origin crust subducts and decreased plate coupling (lower σ_a) along the southern portion where CNS origin Cocos Plate subducts. These trends are consistent with other seismic and geodetic estimates of plate locking for the region, as well as with estimates of fault maturity based on past displacements. One exception to the decreasing along-strike trend in σ_a is the high σ_a event near the region of the 1990 M_w = 7.0 earthquake that may represent an area of seamount contact with the upper plate. This suggests that seamount contacts are zones of increased plate coupling similar to results in Japan.

Acknowledgments

[43] Constructive reviews from three anonymous reviewers significantly improved the manuscript. This work was supported by LANL and NSF award OCE-0751610 to SLB.

References

Abercrombie, R. E., M. Antolik, K. Felzer, and G. Ekström (2001), The 1994 Java tsunami earthquake: Slip over a subducting seamount, *J. Geophys. Res.*, *106*(B4), 6595–6607, doi:10.1029/2000JB900403.

Aki, K. (1969), Analysis of the seismic coda of local earthquakes as scattered waves, *J. Geophys. Res.*, *74*(2), 615–631, doi:10.1029/JB074i002p00615.

Aki, K., and B. Chouet (1975), Origin of coda waves: Source, attenuation, and scattering effects, *J. Geophys. Res.*, *80*(23), 3322–3342, doi:10.1029/JB080i023p03322.

Allmann, B. P., and P. M. Shearer (2009), Global variations of stress drop for moderate to large earthquakes, *J. Geophys. Res.*, *114*, B01310, doi:10.1029/2008JB005821.

Avants, M., et al. (2001), Large underthrusting earthquakes beneath the Nicoya Peninsula, Costa Rica, *Eos Trans. AGU*, *82*(47), Fall Meet. Suppl., Abstract T52E-07.

Bangs, N. L. B., S. P. S. Gulick, and T. H. Shipley (2006), Seamount subduction erosion in the Nankai Trough and its potential impact on the seismogenic zone, *Geology*, *34*(8), 701–704, doi:10.1130/G22451.1.

Barckhausen, U., C. R. Ranero, R. von Huene, S. C. Cande, and H. A. Roeser (2001), Revised tectonic boundaries in the Cocos Plate off Costa Rica: Implications for the segmentation of the convergent margin and for plate tectonics, *J. Geophys. Res.*, *106*(B9), 19,207–19,220, doi:10.1029/2001JB000238.

Bilek, S. L., S. Y. Schwartz, and H. R. DeShon (2003a), Control of seafloor roughness on earthquake rupture behavior, *Geology*, *31*(5), 455–458, doi:10.1130/0091-7613(2003)031<0455:COSROE>2.0.CO;2.

Bilek, S. L., L. Ruff, H. R. DeShon, S. Y. Schwartz, and A. V. Newman (2003b), Comparison of earthquake focal mechanisms and source processes along Nicoya and Osa Peninsulas, Costa Rica, paper presented at The Seismogenic Zone Experiment (SEIZE) Revisited, MARGINS Theor. Inst., Snowbird, Utah.

Brune, J. N. (1970), Tectonic stress and the spectra of seismic shear waves from earthquakes, *J. Geophys. Res.*, *75*(26), 4997–5009, doi:10.1029/JB075i026p04997.

Bürgmann, R., et al. (2005), Interseismic coupling and asperity distribution along the Kamchatka subduction zone, *J. Geophys. Res.*, *110*, B07405, doi:10.1029/2005JB003648.

Chouet, B., K. Aki, and M. Tsujiura (1978), Regional variation of the scaling law of earthquake source spectra, *Bull. Seismol. Soc. Am.*, *68*(1), 49–79.

Choy, G. L., and J. L. Boatwright (1995), Global patterns of radiated seismic energy and apparent stress, *J. Geophys. Res.*, *100*(B9), 18,205–18,228, doi:10.1029/95JB01969.

Choy, G. L., and S. H. Kirby (2004), Apparent stress, fault maturity and seismic hazard for normal-fault earthquakes at subduction zones, *Geophys. J. Int.*, *159*(3), 991–1012, doi:10.1111/j.1365-246X.2004.02449.x.

Choy, G. L., A. McGarr, S. H. Kirby, and J. Boatwright (2006), An overview of the global variability in radiated energy and apparent stress, in *Earthquakes: Radiated Energy and the Physics of Faulting*, *Geophys. Monogr. Ser.*, vol. 170, edited by R. Abercrombie et al., pp. 43–57, AGU, Washington, D. C.

Cloos, M. (1992), Thrust-type subduction-zone earthquakes and seamount asperities: A physical model for seismic rupture, *Geology*, *20*, 601–604, doi:10.1130/0091-7613(1992)020<0601:TTSZEA>2.3.CO;2.

DeShon, H. R., et al. (2006), Seismogenic zone structure beneath the Nicoya Peninsula, Costa Rica, from 3D local earthquake *P*- and *S*-wave tomography, *Geophys. J. Int.*, *164*, 109–124, doi:10.1111/j.1365-246X.2005.02809.x.

Dominguez, S., J. Malavieille, and S. E. Lallemand (2000), Deformation of accretionary wedges in response to seamount subduction: Insights from sandbox experiments, *Tectonics*, *19*(1), 182–196, doi:10.1029/1999TC900055.

Eken, T., et al. (2004), An application of the coda methodology for moment-rate spectra using broadband stations in Turkey, *Geophys. Res. Lett.*, *31*, L11609, doi:10.1029/2004GL019627.

Fisher, D. M., T. W. Gardner, J. S. Marshall, P. B. Sak, and M. Protti (1998), Effects of subducting sea-floor roughness on fore-arc kinematics, Pacific coast, Costa Rica, *Geology*, *26*(5), 467–470, doi:10.1130/0091-7613(1998)026<0467:EOSSFR>2.3.CO;2.

Fisher, A. T., et al. (2003), Abrupt thermal transition reveals hydrothermal boundary and role of seamounts within the Cocos Plate, *Geophys. Res. Lett.*, *30*(11), 1550, doi:10.1029/2002GL016766.

Gardner, T., et al. (2001), Holocene forearc block rotation in response to seamount subduction, southeastern Peninsula de Nicoya, Costa Rica, *Geology*, *29*(2), 151–154, doi:10.1130/0091-7613(2001)029<0151:HFBRIR>2.0.CO;2.

Ghosh, A., A. V. Newman, A. M. Thomas, and G. T. Farmer (2008), Interface locking along the subduction megathrust from *b* value mapping near Nicoya Peninsula, Costa Rica, *Geophys. Res. Lett.*, *35*, L01301, doi:10.1029/2007GL031617.

Gonzalez, V., and L. Persson (1997), Regional coda *Q* in Costa Rica, Central America, *J. Seismol.*, *1*, 269–287, doi:10.1023/A:1009777605524.

Güendel, F., et al. (1989), First results from a new seismographic network in Costa Rica, Central America, *Bull. Seismol. Soc. Am.*, *79*(1), 205–210.

Hansen, S. E., S. Y. Schwartz, H. R. DeShon, and V. González (2006), Earthquake relocation and focal mechanisms determination using waveform cross correlation, Nicoya Peninsula,

Costa Rica, *Bull. Seismol. Soc. Am.*, *96*(3), 1003–1011, doi:10.1785/0120050129.

Harris, R. N., and K. Wang (2002), Thermal models of the Middle America Trench at the Nicoya Peninsula, Costa Rica, *Geophys. Res. Lett.*, *29*(21), 2010, doi:10.1029/2002GL015406.

Harris, R. N., et al. (2010a), Thermal regime of the Costa Rican convergent margin: 1. Along-strike variations in heat flow from probe measurements and estimated from bottom-simulation reflectors, *Geochem. Geophys. Geosyst.*, *11*, Q12S28, doi:10.1029/2010GC003272.

Harris, R. N., et al. (2010b), Thermal regime of the Costa Rican convergent margin: 2. Thermal models of the shallow Middle America subduction zone offshore Costa Rica, *Geochem. Geophys. Geosyst.*, *11*, Q12S29, doi:10.1029/2010GC003273.

Hey, R. (1977), Tectonic evolution of the Cocos-Nazca spreading center, *Geol. Soc. Am. Bull.*, *88*, 1404–1420, doi:10.1130/0016-7606(1977)88<1404:TEOTCS>2.0.CO;2.

Hinz, K., R. von Huene, and C. R. Ranero (1996), Tectonic structure of the convergent Pacific margin offshore Costa Rica from multichannel seismic reflection data, *Tectonics*, *15*(1), 54–66, doi:10.1029/95TC02355.

Husen, S., E. Kissling, and R. Quintero (2002), Tomographic evidence for subducted seamount beneath the Gulf of Nicoya, Costa Rica: The cause of the 1990 M_w = 7.0 Gulf of Nicoya earthquake, *Geophys. Res. Lett.*, *29*(8), 1238, doi:10.1029/2001GL014045.

Husen, S., R. Quintero, E. Kissling, and B. Hacker (2003), Subduction-zone structure and magmatic processes beneath Costa Rica constrained by local earthquake tomography and petrological modeling, *Geophys. J. Int.*, *155*(1), 11–32, doi:10.1046/j.1365-246X.2003.01984.x.

Kanamori, H., and L. Rivera (2004), Static and dynamic scaling relations for earthquakes and their implications for rupture speed and stress drop, *Bull. Seismol. Soc. Am.*, *94*(1), 314–319, doi:10.1785/0120030159.

LaFemina, P., et al. (2009), Fore-arc motion and Cocos ridge collision in Central America, *Geochem. Geophys. Geosyst.*, *10*, Q05S14, doi:10.1029/2008GC002181.

Lundgren, P., et al. (1999), Seismic cycle and plate margin deformation in Costa Rica: GPS observations from 1994 to 1997, *J. Geophys. Res.*, *104*(B12), 28,915–28,926, doi:10.1029/1999JB900283.

Malagnini, L., K. Mayeda, A. Akinci, and P. L. Bragato (2004), Estimating absolute site effects, *Bull. Seismol. Soc. Am.*, *94*(4), 1343–1352, doi:10.1785/012003161.

Malagnini, L., P. Bodin, K. Mayeda, and A. Akinci (2006), Unbiased moment-rate spectra and absolute site effects in the Kachchh basin, India, from the analysis of the aftershocks of the 2001 M_w 7.6 Bhuj earthquake, *Bull. Seismol. Soc. Am.*, *96*(2), doi:10.1785/0120050089.

Marshall, J. S., and R. S. Anderson (1995), Quaternary uplift and seismic cycle deformation, Peninsula de Nicoya, Costa Rica, *Geol. Soc. Am. Bull.*, *107*(4), 463–473, doi:10.1130/0016-7606(1995)107<0463:QUASCD>2.3.CO;2.

Mayeda, K. (1993), mb(LgCoda): A stable single station estimator of magnitude, *Bull. Seismol. Soc. Am.*, *83*(3), 851–861.

Mayeda, K., and L. Malagnini (2009), Apparent stress and corner frequency variations in the 1999 Taiwan (Chi-Chi) sequence: Evidence for a step-wise increase at M_w ~ 5.5, *Geophys. Res. Lett.*, *36*, L10308, doi:10.1029/2009GL037421.

Mayeda, K., and W. R. Walter (1996), Moment, energy, stress drop, and source spectra of western United States earthquakes from regional coda envelopes, *J. Geophys. Res.*, *101*(B5), 11,195–11,208, doi:10.1029/96JB00112.

Mayeda, K., A. Hofstetter, J. L. O'Boyle, and W. R. Walter (2003), Stable and transportable regional magnitudes based on coda-derived moment-rate spectra, *Bull. Seismol. Soc. Am.*, *93*(1), 224–239, doi:10.1785/0120020020.

Mayeda, K., R. Gok, W. R. Walter, and A. Hofstetter (2005), Evidence for non-constant energy/moment scaling from coda-derived source spectra, *Geophys. Res. Lett.*, *32*, L10306, doi:10.1029/2005GL022405.

Mayeda, K., L. Malagnini, and W. R. Walter (2007), A new spectral ratio method using narrow band coda envelopes: Evidence for non-selfsimilarity in the Hector Mine sequence, *Geophys. Res. Lett.*, *34*, L11303, doi:10.1029/2007GL030041.

McGarr, A. (1999), On relating apparent stress to the stress causing earthquake fault slip, *J. Geophys. Res.*, *104*(B2), 3003–3011, doi:10.1029/1998JB900083.

Mochizuki, K., T. Yamada, M. Shinohara, Y. Yamanaka, and T. Kanazawa (2008), Weak interface coupling by seamounts and repeating M ~ 7 earthquakes, *Science*, *321*, 1194–1197, doi:10.1126/science.1160250.

Newman, A. V., and E. A. Okal (1998), Teleseismic estimates of radiated seismic energy: The E/M_0 discriminant for tsunami earthquakes, *J. Geophys. Res.*, *103*(B11), 26,885–98, doi:10.1029/98JB02236.

Newman, A. V., et al. (2002), Along-strike variability in the seismogenic zone below Nicoya Peninsula, Costa Rica, *Geophys. Res. Lett.*, *29*(20), 1977, doi:10.1029/2002GL015409.

Nishenko, S. P. (1991), Circum-Pacific seismic potential: 1989–1999, *Pure Appl. Geophys.*, *135*(2), 169–259, doi:10.1007/BF00880240.

Norabuena, E., et al. (2004), Geogedic and seismic constraints on some seismogenic zone processes in Costa Rica, *J. Geophys. Res.*, *109*, B11403, doi:10.1029/2003JB002931.

Outerbridge, K. C., et al. (2010), A tremor and slip event on the Cocos-Caribbean subduction zone as measured by a global positioning system (GPS) and seismic network on the Nicoya Peninsula, Costa Rica, *J. Geophys. Res.*, *115*, B10408, doi:10.1029/2009JB006845.

Phillips, W. S., and K. Aki (1986), Site amplification of coda waves from local earthquakes in central California, *Bull. Seismol. Soc. Am.*, *76*(3), 627–648.

Phillips, W. S., R. J. Stead, G. E. Randall, H. E. Hartse, and K. M. Mayeda (2008), Source effects from broad area network calibration of regional distance coda waves, *Adv. Geophys.*, *50*, 319–351.

Phillips, W. S., X. Yang, R. J. Stead, M. L. Begnaud, and K. M. Mayeda (2010), Model Development for broad area event identification and yield estimation, paper presented at Monitoring Research Review 2010, Orlando Fla., 21–23 Sept.

Press, W. H., S. A. Teukolsky, W. T. Vetterling, and B. P. Flannery (Eds.) (2007), *Numerical Recipes: The Art of Scientific Computing*, Cambridge Univ. Press, New York.

Prieto, G. A., P. M. Shearer, F. L. Vernon, and D. Kilb (2004), Earthquake source scaling and self-similarity estimation from stacking P and S spectra, *J. Geophys. Res.*, *109*, B08310, doi:10.1029/2004JB003084.

Protti, M., et al. (1995), The March 25, 1990 (M_w = 7.0, M_L = 6.8), earthquake at the entrance of the Nicoya Gulf, Costa Rica: Its prior activity, foreshocks, aftershocks, and triggered seismicity, *J. Geophys. Res.*, *100*(B10), 20,345–20,358, doi:10.1029/94JB03099.

Ranero, C. R., and R. von Huene (2000), Subduction erosion along the Middle America convergent margin, *Nature*, *404*, 748–752, doi:10.1038/35008046.

Ranero, C. R., J. P. Morgan, K. McIntosh, and C. Reichert (2003), Bending-related faulting and mantle serpentinization

at the Middle America trench, *Nature*, *425*, 367–373, doi:10.1038/nature01961.

Rautian, T. G., and V. I. Khalturin (1978), The use of the coda for determination of the earthquake source spectrum, *Bull. Seismol. Soc. Am.*, *68*(4), 923–948.

Robinson, D. P., S. Das, and A. B. Watts (2006), Earthquake rupture stalled by a subducting fracture zone, *Science*, *312*(5777), 1203–1205, doi:10.1126/science.1125771.

Ruff, L. J. (1989), Do trench sediments affect great earthquake occurrence in subduction zones?, *Pure Appl. Geophys.*, *129*, 263–282, doi:10.1007/BF00874629.

Ryan, H. F., and D. W. Scholl (1993), Geological implications of great interplate earthquakes along the Aleutian arc, *J. Geophys. Res.*, *98*, 22,135–22,146, doi:10.1029/93JB02451.

Sak, P. B., D. M. Fisher, T. W. Gardner, J. S. Marshall, and P. C. LaFemina (2009), Rough crust subduction, forearc kinematics, and Quaternary uplift rates, Costa Rican segment of the Middle American Trench, *Geol. Soc. Am. Bull.*, *121*, 992–1012, doi:10.1130/B26237.1.

Scholz, C. H. (2002), *The Mechanics of Earthquakes and Faulting*, 2nd ed., Cambridge Univ. Press, Cambridge, U. K.

Scholz, C. H., and C. Small (1997), The effect of seamount subduction on seismic coupling, *Geology*, *25*(6), 487–490, doi:10.1130/0091-7613(1997)025<0487:TEOSSO>2.3.CO;2.

Schorlemmer, D., and S. Wiemer (2005), Microseismicity data forecast rupture area, *Nature*, *434*, 1086, doi:10.1038/4341086a.

Silver, E., et al. (2000), Fluid flow paths in the Middle America Trench and Costa Rica margin, *Geology*, *28*(8), 679–682, doi:10.1130/0091-7613(2000)28<679:FFPITM>2.0.CO;2.

Spinelli, G. A., and D. M. Saffer (2004), Along-strike variations in underthurst sediment dewatering on the Nicoya margin, Costa Rica related to the updip limit of seismicity, *Geophys. Res. Lett.*, *31*, L04613, doi:10.1029/2003GL018863.

Spinelli, G. A., D. M. Saffer, and M. B. Underwood (2006), Hydrogeologic responses to three-dimensional temperature variability, Costa Rica subduction margin, *J. Geophys. Res.*, *111*, B04403, doi:10.1029/2004JB003436.

Taylor, S. R., and H. E. Hartse (1998), A procedure for estimation of source and propagation amplitude corrections for regional seismic discriminants, *J. Geophys. Res.*, *103*(B2), 2781–2789, doi:10.1029/97JB03292.

Tristan, D. J. F. (1916), The Costa Rica earthquake of February 27, 1916, *Bull. Seismol. Soc. Am.*, *6*(4), 232–235.

von Huene, R. (2008), When seamounts subduct, *Science*, *321*, 1165–1166, doi:10.1126/science.1162868.

von Huene, R., C. R. Ranero, and W. Weinrebe (2000), Quaternary convergent margin tectonics of Costa Rica, segmentation of the Cocos Plate, and Central American volcanism, *Tectonics*, *19*(2), 314–334, doi:10.1029/1999TC001143.

Walter, W. R., and S. R. Taylor (2001), A revised magnitude and distance amplitude correction (MDAC2) procedure for regional seismic discriminants: Theory and testing at NTS, *Rep. UCRL-ID-146*882, 16 pp., Lawrence Livermore Natl. Lab., Livermore, Calif.

Walter, W. R., et al. (2007), Regional body-wave attenuation using a coda source normalization method: Application to MEDNET records of earthquakes in Italy, *Geophys. Res. Lett.*, *34*, L10308, doi:10.1029/2007GL029990.

Wyss, M., and P. Molnar (1972), Efficiency, stress drop, apparent stress, effective stress, and frictional stress of Denver, Colorado, earthquakes, *J. Geophys. Res.*, *77*(8), 1433–1438, doi:10.1029/JB077i008p01433.

Ye, S., et al. (1996), Crustal structure of the Middle American Trench off Costa Rica from wide-angle seismic data, *Tectonics*, *15*(5), 1006–1021, doi:10.1029/96TC00827.